

Observational constraints on dark matter decaying via gravity portals

Sun Xu-Dong and Dai Ben-Zhong¹

School of Physics and Astronomy, Yunnan University, Kunming, 650091, China

Key Laboratory of Astroparticle Physics, Yunnan Province, Kunming 650091, China.

E-mail: bestsunxudong@126.com, bzhdai@ynu.edu.cn

ABSTRACT: Global symmetry can guarantee the stability of dark matter particles (DMPs). However, the nonminimal coupling between dark matter (DM) and gravity can destroy the global symmetry of DMPs, which in turn leads to their decay. Under the framework of nonminimal coupling between scalar singlet dark matter (ssDM) and gravity, it is worth exploring to what extent the symmetry of ssDM is broken. It is suggested that the total amount of decay products of ssDM cannot exceed current observational constraints. Along these lines, the data obtained with satellites such as Fermi-LAT and AMS-02 can limit the strength of the global symmetry breaking of ssDM. Since the mass of many well motivated DM candidates may be in the GeV–TeV range, we determine a reasonable parameter range for the lifetime in this range. We find that when the mass of the ssDM is around the electroweak scale (246 GeV), the corresponding $3\text{-}\sigma$ lower limits of the lifetime of ssDM is 5.3×10^{26} s. Our analysis of ssDM around the typical electroweak scale contains the most abundant decay channels of all mass range, so the analysis of the behavior of ssDM under the influence of gravity is more comprehensive.

KEYWORDS: Cosmology of Theories beyond the SM, Dark Matter, Beyond Standard Model

PACS: 95.35.+d, 95.30.Cq

ARXIV EPRINT: [2002.09955](https://arxiv.org/abs/2002.09955)

¹Corresponding author.

Contents

1	Introduction	1
2	The Model and Branch Ratio	3
2.1	The Model	3
2.2	Branch Ratio	4
3	Decay spectrum induced by global symmetry breaking	6
3.1	Decay spectrum at production	6
3.2	Fluxes after propagation	8
4	Constraints from isotropic diffuse γ-ray background (IGRB) and the cosmic positron spectrum	10
4.1	Statistic methods to set constraints	10
4.2	Treatment of the background	10
5	Results	11
6	Discussion and Conclusions	14

1 Introduction

Observations of the rotation curves of galaxies, the Bullet Cluster, gravitationally lensed galaxy clusters, type Ia supernovae, baryonic acoustic oscillations, and anisotropies in the cosmic microwave background have all implied the existence of dark matter (DM) [1]. The Standard Model of particle physics describes electromagnetism, as well as the weak and strong nuclear forces successfully [2], however it does not currently accommodate the existence of any dark matter particles (DMPs). All these imply that physics beyond the Standard Model should be in place [3] [4].

Among the various properties of DMPs, we are concerned with their stability, because if DMPs are unstable, we could observe their decay products with satellites [5] [6] [7]. The stability of electrons is guaranteed by electric charge conservation, while the stability of neutrinos is guaranteed by Lorentz symmetry. Similarly, current observations have suggested that DM is stable and may be composed of particles. It is usually assumed that DMPs have global symmetry in Minkowski space-time, such as the hypothetical Z_2 symmetry [8] [9]. But every particle is subject to gravitational interactions. In reality, there is no Minkowski space-time, and gravity does not necessarily couple to DM minimally. In the minimal coupling regime, matter distribution decides the distribution of gravitons, and gravitons and matter do not transform each other. However, if gravitons couples to DM nonminimally, the global symmetry of DMPs can be broken [10] [11]. Consequently, the

stability of DMPs is no longer preserved under the influence of gravity [12] [13] [14] [15], implying that DMPs could decay via nonminimal coupling due to gravity.

Catà et al. [16] [23] give such models of scalar singlet dark matter (ssDM), inert doublet DM and fermionic DM with global symmetry breaking induced by nonminimal coupling to gravity. There were also other attempts to study the nonminimal coupling regime. For example, the Higgs field may have nonminimal coupling with gravity in Higgs inflation [17]. If the mass of the dark matter particle (DMP) is less than 270 MeV, such a particle could concurrently be acting as an inflaton [18]. There are also nonminimal coupling models of DM and gravity where the global symmetry is not destroyed by gravity [19] [20]. As both an inflaton and DMP, the nonminimal coupling between a complex scalar field and gravity has also been used to explain the electroweak phase transition [21] [22].

Many observations and experiments could set limits on the strength of the global symmetry breaking of DMPs. Currently, there are many types of experiments and observational methods being used to search for DMPs. Direct detection methods rely on monitoring nucleon recoil induced by interactions with DMPs distributed around the Earth [24]. Indirect detection methods search for photons, neutrinos, and/or cosmic rays produced by DMPs using satellites and Earth-based instrumentation [25]. The Large Hadron Collider (LHC) also serves as a complementary experiment in the search for DM. Cosmological studies have also provided constraints on DM. If nonminimal coupling to gravity breaks the global symmetry of DMPs, DM would be unstable, and it would consequently decay into observable particles such as cosmic rays [26], neutrinos [27] or cosmic gamma-rays [28]. So while no conclusive particle signal has yet been attributed to DM [29], current observations can still be used to set limits on the stability of DMP.

Using chiral perturbation theory, Catà et al. [30] provided the allowed parameter space of light ssDM particles less massive than 1 GeV, in which the decay products have a sharp photon spectrum. These authors obtained the strongest restriction to date using Fermi-LAT gamma-ray observations. However, the mass range of weakly interacting massive particles (WIMP) and super WIMPs proposed based on the gauge hierarchy problem as well as hidden DM based on the gauge hierarchy problem and new flavour physics is expected to be GeV–TeV [31]. And, if the mass of the DMP is in the GeV–TeV range, more decay channels will be opened and the decay properties of DMPs will be quite diverse. Assuming that the lifetime of DMPs is longer than the age of the universe and using observation data from neutrino telescopes, Catà et al. [16] [23] provided rough restrictions of the nonminimal coupling coefficient between the ssDM, the inert doublet DM, the fermionic DM and the gravitons around the GeV–TeV range.

In the case of DM decay, constraints obtained via indirect-detection methods play an important role. As indirect-detection methods, satellites such as Fermi-LAT [32], Alpha Magnetic Spectrometer (AMS) [33], and Dark Matter Particle Explorer (DAMPE) [34] can obtain sensitive observations of high-energy photons and cosmic rays. However, DAMPE is unable to distinguish between positrons and electrons, thus in this current work we only consider positron data obtained by AMS-02 [33] and photon data obtained by Fermi-LAT [32] to yield conservative indirect restrictions of the GeV–TeV range.

According to the work of Catà et al. [23], the action is constructed in the Jordan frame.

When using Feynman diagrams to calculate the specific decay channel, one can choose to calculate it in either Jordan frame or Einstein frame. For example, Ren et al. [35] used the quantum field theory method to calculate Higgs inflation both in Jordan frame and Einstein frame. They obtained the same result using both, which reflects the equivalence of the Jordan frame and the Einstein frame in these scenarios. Then, in the Einstein frame, we calculate the spectra of photons and positrons arising from the decay of ssDM particles in the GeV–TeV range where WIMPs, super WIMPs and hidden DM mass may likely be. Finally, we obtain constraints on the lifetime and the nonminimal coupling constant ξ , which reflects the strength of the global symmetry breaking of ssDM particles, by comparing our theoretical spectra to observations made by Fermi-LAT and AMS-02.

The structure of this paper is as follows. In Section 2, we introduce the model and discussed the decay branch ratio of ssDM around the electroweak scale. In Section 3, we describe the calculation of the ssDM decay spectrum induced by global symmetry breaking. In Section 4, we show the statistic methods to compare the expected spectrum from decaying ssDM with the observed spectrum from Fermi-LAT and AMS-02. In Section 5, we give decay spectra of ssDM induced by global symmetry breaking and the reasonable parameter space of the lifetime and the nonminimal coupling constant. The discussion and conclusions are presented in Section 6.

2 The Model and Branch Ratio

2.1 The Model

Catà et al. [16] considered that DM has a nonminimal coupling with gravity and whose global symmetry is broken in curved space-time. In this paper, we focus on ssDM. In Jordan Frame, the action \mathcal{S} of system can be written as (2.1):

$$\mathcal{S} = \int d^4x \sqrt{-g} \left[-\frac{R}{2\kappa^2} + \mathcal{L}_{SM} + \mathcal{L}_{DM} - \xi M \varphi R \right] \quad (2.1)$$

where g is the determinant of metric tensor $g_{\mu\nu}$.

The Einstein–Hilbert Lagrangian $-R/2\kappa^2$ describes the gravitational sector, where R is the Ricci scalar and $\kappa = \sqrt{8\pi G}$ is the inverse (reduced) Planck mass with G the Newtonian gravitational constant.

\mathcal{L}_{SM} is the Standard Model Lagrangian. It accurately describes the electromagnetism, weak and strong nuclear forces at energies around the electroweak scale and could be cast as,

$$\mathcal{L}_{SM} = \mathcal{T}_F + \mathcal{T}_f + \mathcal{T}_H + \mathcal{L}_Y - \mathcal{V}_H \quad (2.2)$$

where \mathcal{V}_H is the Higgs potential, \mathcal{L}_Y is the Yukawa interaction term and \mathcal{T}_i are the kinetic terms of spin–one particles, fermions and scalars,

$$\mathcal{T}_F = -\frac{1}{4} g^{\mu\nu} g^{\lambda\rho} F_{\mu\lambda}^a F_{\nu\rho}^a \quad (2.3a)$$

$$\mathcal{T}_f = \frac{i}{2} \bar{f} \overleftrightarrow{\nabla} f \quad (2.3b)$$

$$\mathcal{T}_H = g^{\mu\nu}(D_\mu\phi)^\dagger(D_\nu\phi). \quad (2.3c)$$

In these equations, the slashed derivative operator is defined as $\not{\nabla} = \gamma^a e_a^\mu \nabla_\mu$, where $\nabla_\mu = D_\mu - \frac{i}{4} e_\nu^b (\partial_\mu e^{\nu c}) \sigma_{bc}$ and $e^{\nu c}$ the vierbein. D_μ represents the gauge covariant derivative. ϕ denotes the Higgs doublet.

In Eq. (2.1), $\mathcal{L}_{DM} = \mathcal{T}_\varphi - V(\varphi, X)$ is the Lagrangian of the ssDM, where φ represents ssDM. $V(\varphi, X)$ is the DM potential. Since the DM potential contains interactions between ssDM and Standard Model particles X , it could be responsible for the correct DM relic abundance.

The research content of this paper comes from the last term of Eq. (2.1). Specifically, $-\xi M \varphi R$ is the assumed non-minimal coupling operator between the ssDM and gravity, where ξ is the coupling constant, M is a parameter with dimension one so that ξ is dimensionless. For convenience, we fix $M = \kappa^{-1}$. This non-minimal coupling operator breaks global \mathbb{Z}_2 symmetry of φ , consequently induces ssDM decay into Standard Model particles.

Using conformal transformation, as shown in Eq. (2.4):

$$\tilde{g}_{\mu\nu} = \Omega^2 g_{\mu\nu} \quad (2.4)$$

where $\Omega^2 = 1 + 2\xi M \kappa^2 \varphi$, one can acquire action in Einstein Frame, which is shown as Eq. (2.5):

$$\mathcal{S} = \int d^4x \sqrt{-\tilde{g}} \left[-\frac{\tilde{R}}{2\kappa^2} + \frac{3}{\kappa^2} \frac{\Omega_{,\rho} \tilde{\Omega}^{,\rho}}{\Omega^2} + \tilde{\mathcal{L}}_{SM} + \tilde{\mathcal{L}}_{DM} \right] \quad (2.5)$$

where:

$$\tilde{\mathcal{L}}_{SM} = \tilde{\mathcal{T}}_F + \Omega^{-3} \tilde{\mathcal{T}}_f + \Omega^{-2} \tilde{\mathcal{T}}_H + \Omega^{-4} (\mathcal{L}_Y - \mathcal{V}_H) \quad (2.6)$$

and $\tilde{\mathcal{L}}_{DM} = \tilde{\mathcal{T}}_\varphi / \Omega^2 - V(\varphi, X) / \Omega^4$. In these expressions, all tilded quantities are formed from $\tilde{g}_{\mu\nu}$.

Eq. (2.6) indicates that DM φ could decay or annihilate into Standard Model particles through gravity portals. Taylor expansion of Eq. (2.6) with respect to ξ shows that the dominant term is the decay term, as shown in Eq. (2.7):

$$\tilde{\mathcal{L}}_{SM,\varphi} = -2\kappa\xi\varphi \left[\frac{3}{2} \tilde{\mathcal{T}}_f + \tilde{\mathcal{T}}_H + 2(\mathcal{L}_Y - \mathcal{V}_H) \right] \quad (2.7)$$

Using Eq. (2.7), Catà et al. [23] gave Feynman rules for DM decay, as shown in Table 1.

2.2 Branch Ratio

Following the procedure provided by Catà et al. [16], we draw decay branch ratios of the ssDM, which is shown in Fig. 1. And Catà et al. also provided the asymptotic dependence of the corresponding partial width on the ssDM mass, in the limit of the massless final-state Standard Model particles, as shown in Table 2. This work focuses on the ssDM with a mass around the electroweak scale.

Below the electroweak scale ($m_\varphi < v$), decay branch ratio is dominated by $\varphi \rightarrow q\bar{q}g$ channel. Although the asymptotic scaling of $\varphi \rightarrow f\bar{f}\gamma$ channel is also m_φ^3 , this channel is suppressed by α_{em}/α_s . Compared with $\varphi \rightarrow q\bar{q}g$ channel, $\varphi \rightarrow f\bar{f}h$ channel is suppressed by m_f^2/v^2 . The ratio of $\varphi \rightarrow f\bar{f}$ channel to $\varphi \rightarrow q\bar{q}g$ channel is m_f^2/m_φ^2 . Therefore, when

Table 1. Feynman rules for DM decay

terms from $\tilde{\mathcal{L}}_{sm,\varphi}$ (2.7)	physical process	Feynman rules
$\xi\kappa m_{f_i}\varphi\bar{f}_if_i$	$\varphi \rightarrow \bar{f}_i, f_i$	$i\xi\kappa m_{f_i}$
$-3\xi\kappa\varphi Y_\mu\bar{f}_i(\gamma^a e_a^\mu)(a_{f_{ij}} - b_{f_{ij}}\gamma^5)f_j$	$\varphi \rightarrow Y_\mu, \bar{f}_i, f_j$	$-3i\xi\kappa(\gamma^a e_a^\mu)(a_{f_{ij}} - b_{f_{ij}}\gamma^5)$
$-\xi\kappa\varphi[(\partial_\mu h)^2 - 2m_h^2 h^2]$	$\varphi \rightarrow h, h$	$2i\xi\kappa[p_{1\mu}p_2^\mu + 2m_h^2]$
$-\xi\kappa\varphi[2m_W^2 W^{\mu+}W_\mu^- + m_Z^2 Z^\mu Z_\mu]$	$\varphi \rightarrow Y_\mu, Y_\nu$	$-2i\xi\kappa m_{Y_\mu}^2 \tilde{g}^{\mu\nu}$
$-2\xi\kappa\varphi\frac{h}{v}[2m_W^2 W^{\mu+}W_\mu^- + m_Z^2 Z^\mu Z_\mu]$	$\varphi \rightarrow h, Y_\mu, Y_\nu$	$-4i\xi\kappa\frac{1}{v}m_{Y_\mu}^2 \tilde{g}^{\mu\nu}$
$-\xi\kappa\varphi\frac{h^2}{v^2}[2m_W^2 W^{\mu+}W_\mu^- + m_Z^2 Z^\mu Z_\mu]$	$\varphi \rightarrow h, h, Y_\mu, Y_\nu$	$-4i\xi\kappa\frac{1}{v^2}m_{Y_\mu}^2 \tilde{g}^{\mu\nu}$
$4\xi\kappa\varphi m_{f_i}\bar{f}_if_i\frac{h}{v}$	$\varphi \rightarrow h, \bar{f}_i, f_i$	$4i\xi\kappa\frac{m_{f_i}}{v}$
$2\xi\kappa\frac{m_h^2}{v}\varphi h^3$	$\varphi \rightarrow h, h, h$	$12i\xi\kappa\frac{m_h^2}{v}$
$\frac{1}{2}\xi\kappa\frac{m^2}{v^2}\varphi h^4$	$\varphi \rightarrow h, h, h, h$	$12i\xi\kappa\frac{m_h^2}{v^2}$

In the table, f_i represents a fermion and index i includes all fermion flavours, Y_μ represents a spin-one particle, $a_{f_{ij}}$ and $b_{f_{ij}}$ can be obtained from the expansion of $\tilde{\mathcal{T}}_f$. W^μ represents the W boson and Z^μ represents the Z boson, h represents the Higgs boson, $v = 246.2$ GeV is the Higgs vacuum expectation value, m_{Y_μ} represents the mass of the spin-one particle, m_{f_i} represents the mass of the fermion, m_h represents the mass of the Higgs boson. The second column lists the decay channels. For example, $\varphi \rightarrow \bar{f}_i, f_i$ represents the channel through which DM φ decays into a pair of fermions.

Table 2. Tree-level decay modes of the ssDM [16]

Decay mode	Asymptotic scaling
$\varphi \rightarrow hh, WW, ZZ$	m_φ^3
$\varphi \rightarrow f\bar{f}$	$m_\varphi m_f^2$
$\varphi \rightarrow hhh$	$m_\varphi v^2$
$\varphi \rightarrow WW h, ZZ h$	m_φ^5/v^2
$\varphi \rightarrow f\bar{f}h$	$m_\varphi^3 m_f^2/v^2$
$\varphi \rightarrow f'\bar{f}'W, f\bar{f}Z$	m_φ^5/v^2
$\varphi \rightarrow f f\gamma, q\bar{q}g$	m_φ^3
$\varphi \rightarrow hhhh$	m_φ^3
$\varphi \rightarrow WW hh, ZZ hh$	m_φ^7/v^4

the mass of fermions is close to that of ssDM, the contribution of $\varphi \rightarrow f\bar{f}$ channel can not be ignored. It is logical to recognize that in Fig. 1, final-state particles of the hump around 10 GeV of $\varphi \rightarrow f\bar{f}$ channel are mainly tau leptons, charm quarks and bottom quarks, and final-state particles of the peak near 500 GeV are mainly top quarks.

Above the electroweak scale ($4\pi v \lesssim m_\varphi \lesssim 10^5$ GeV), decay branch ratio is dominated by $\varphi \rightarrow f'\bar{f}'W + f\bar{f}Z$ channel. Compared with $\varphi \rightarrow f'\bar{f}'W + f\bar{f}Z$ channel, $\varphi \rightarrow q\bar{q}g$ channel is suppressed by factor v^2/m_φ^2 . Similarly, $\varphi \rightarrow hhhh$ channel is suppressed by factor v^4/m_φ^4 . Although the asymptotic scaling of $\varphi \rightarrow WW h + ZZ h$ channel is same as $\varphi \rightarrow f'\bar{f}'W + f\bar{f}Z$ channel, it is suppressed by the smaller phase space.

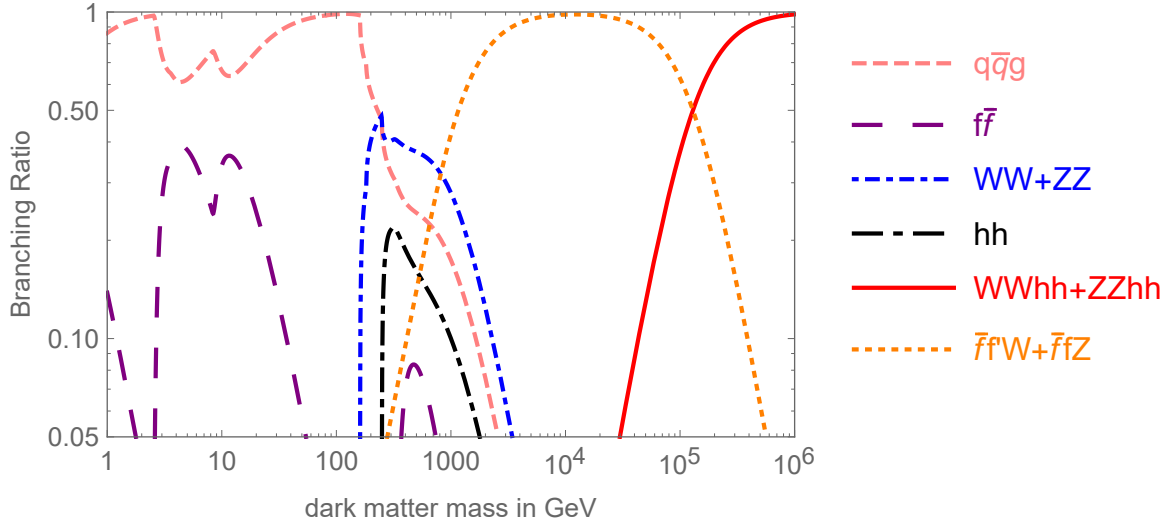


Figure 1. Decay branch ratios of the ssDM via non-minimal coupling to gravity.

Around the electroweak scale ($m_\varphi \sim v$), many channels have the asymptotic scaling of m_φ^3 , including $\varphi \rightarrow WW + ZZ + hh + q\bar{q}g + \bar{f}'f'W + f\bar{f}'Z$. Since the mass of the top quark is also near the electroweak scale, the contribution from $\varphi \rightarrow f\bar{f}$ channel is also can not be neglected. So near the electroweak scale, the decay channels are the most abundant and worth a thorough analysis.

Only channels shown in Fig. 1 were included in the following numerical calculations.

3 Decay spectrum induced by global symmetry breaking

3.1 Decay spectrum at production

Tanabashi et al. (Particle Data Group) [36] provided a detailed procedure to calculate decay rates and decay spectrum at production. These authors gave expressions for differential decay rates, e.g. Eq. (3.1), relativistically invariant three-body phase space, e.g. Eq. (3.2), and relativistically invariant four-body phase space, e.g. Eq. (3.5).

For the convenience of description, in the following, we mark the three product particles arising from three-body decay as particle 1, particle 2 and particle 3. We also use nomenclature for the rest frame of particle i and particle j as F_{ij} .

The expression of the differential decay rate is:

$$d\Gamma = \frac{1}{2m_\varphi} |\mathcal{M}|^2 d\Phi^{(n)}(m_\varphi; p_1, \dots, p_n) \quad (3.1)$$

where Γ is the decay rate of φ in its rest frame, m_φ is mass of the DMP, \mathcal{M} is the invariant matrix element, $\Phi^{(n)}$ is the n -body phase space, and p_i is the four momentum of terminal particle i . We also use the definitions $p_{ij} = p_i + p_j$, $m_{ij}^2 = p_{ij}^2$, so that the element of three body phase space $d\Phi^{(3)}$ can be written as:

$$d\Phi^{(3)} = \frac{1}{2\pi} dm_{12}^2 \frac{1}{16\pi^2} \frac{|\vec{p}_1^*|}{m_{12}} d\Omega_1^* \frac{1}{16\pi^2} \frac{|\vec{p}_3|}{m_\varphi} d\Omega_3 \quad (3.2)$$

where $(|\vec{p}_1^*|, \Omega_1^*)$ is the three momentum of particle 1 in F_{12} , and Ω_3 is the angle of particle 3 in the rest frame of the decaying particle. The symbol $*$ always denotes a quantity in F_{12} .

The relationship between E_3 and m_{12} is:

$$E_3 = \frac{m_\varphi^2 + m_3^2 - m_{12}^2}{2m_\varphi} \quad (3.3)$$

where m_3 and E_3 are the mass and energy of particle 3, respectively. The energy spectrum of particle 3 per decay in a channel with final state l can be calculated following Eq. (3.4):

$$dN^l/dE_3 = \frac{\partial\Gamma^l/\partial E_3}{\Gamma^l} \quad (3.4)$$

Using the vertex rules given in Table 1, and following Eqs. (3.1), (3.2), (3.3) and (3.4), we numerically calculated the decay rate Γ and energy spectrum dN^l/dE_3 . According to translatability symmetry, dN^l/dE_1 and dN^l/dE_2 were also calculated, where E_1 is the energy of particle 1, E_2 is the energy of particle 2.

As for four-body decay, there are three channels: $\varphi \rightarrow W^+, W^-, h, h$; $\varphi \rightarrow Z, Z, h, h$ and $\varphi \rightarrow h, h, h, h$. We will consider $\varphi \rightarrow W^+, W^-, h, h$ here to illustrate our method of calculation. To demonstrate the calculation of Γ and dN^l/dE_1 clearly, we regard the W^+ boson as particle 1 and the W^- boson as particle 2, while the remaining two Higgs bosons are particles 3 and 4. As before, we still denote the rest frame of particles i and j as F_{ij} .

The element of four-body phase space $d\Phi^{(4)}$ can be written as:

$$d\Phi^{(4)} = \frac{1}{2\pi} dm_{12}^2 \frac{1}{2\pi} dm_{34}^2 \frac{1}{16\pi^2} \frac{|\vec{p}_1^*|}{m_{12}} d\Omega_1^* \frac{1}{16\pi^2} \frac{|\vec{p}_3^{**}|}{m_{34}} d\Omega_3^{**} \frac{1}{16\pi^2} \frac{|\vec{p}_{12}|}{m_\varphi} d\Omega_{12} \quad (3.5)$$

where $(|\vec{p}_{12}|, \Omega_{12})$ is the three momentum of p_{12} , and $(\vec{p}_3^{**}, \Omega_3^{**})$ is the three momentum of particle 3 in F_{34} . The symbol $**$ always denotes a quantity in F_{34} . Using Eqs. (3.1) and (3.5), we numerically calculated Γ and $dN^l/(dm_{12}dm_{34})$, where $dN^l = d\Gamma^l/\Gamma^l$. Then we applied Lorentz transformations to $|\vec{p}_1^*|$ and E_1^* . We find that the isotropic spectrum of particle 1 with momentum $|\vec{p}_1^*|$ in F_{12} has a spectrum described by Eq. (3.6) in the rest frame of φ :

$$g(E_1, m_{12}) = \frac{1}{2} \frac{1}{\gamma_{12}\beta_{12}|\vec{p}_1^*|} \Theta(E_1 - E_-) \Theta(E_+ - E_1) \quad (3.6)$$

where β_{ij} is the velocity of F_{ij} relative to the decaying DMP, $\gamma_{ij} = (1 - \beta_{ij}^2)^{-1/2}$, $E_\pm \equiv \gamma_{12}E_1^* \pm \gamma_{12}\beta_{12}|\vec{p}_1^*|$ and $\Theta(x)$ the Heaviside function.

The energy spectrum of particle 1 produced per decay in the channel with final state l can be described by Eq. (3.7):

$$\frac{dN^l}{dE_1} = \int \int g(E_1, m_{12}) \frac{dN^l}{dm_{12}dm_{34}} dm_{12}dm_{34} \quad (3.7)$$

As before, according to translatability symmetry, dN^l/dE_2 , dN^l/dE_3 and dN^l/dE_4 can also be calculated, where E_2 , E_3 and E_4 represent the energy of particles 2, 3 and 4 respectively.

So far, we have obtained many spectra of stable and unstable particles, such as of the Higgs boson, Z boson and neutrino. For comparison with observations, we calculated the spectra of stable particles, including photons and positrons. Cirelli et al. [37] use the PYTHIA codes to generate spectra of photons and positrons $k(E, E_{\gamma, e^+})$ induced by a primary state particle with given energy E , where E_{γ, e^+} represents energy of the photon or positron. The effect of QED and EW Bremsstrahlung are included when they used PYTHIA to generate $k(E, E_{\gamma, e^+})$, while the effects of Inverse Compton processes or synchrotron radiation are not included [37]. Then, the secondary photon or positron energy spectrum produced per decay in a channel with final state l represented by $dN^l/dE_{\gamma, e^+}$ was numerically calculated as:

$$\frac{dN^l}{dE_{\gamma, e^+}} = \sum_s \int k(E_s, E_{\gamma, e^+}) \frac{dN^l}{dE_s} dE_s \quad (3.8)$$

where s includes all final state particles in the channel with final state l . In the three-body decay case, s runs from 1 to 3, while in the four-body decay case s runs from 1 to 4.

3.2 Fluxes after propagation

Finally, the spectra that could be detected by satellites are calculated via PPPC 4 DM ID [37]. In the following, we uniformly adopt the Navarro-Frenk-White (NFW) DM distribution model

$$\rho(r) = \rho_s \frac{r_s}{r} \left(1 + \frac{r}{r_s}\right)^{-2} \quad (3.9)$$

with parameters $\rho_s = 0.184 \text{ GeV/cm}^3$, $r_s = 24.42 \text{ kpc}$, where $\rho(r)$ is energy density of DM.

The differential flux of positrons in space \vec{x} and time t is given by $d\Phi_{e^+}/dE_{e^+}(t, \vec{x}, E_{e^+}) = v_{e^+} f/4\pi$ where v_{e^+} is the velocity of the positrons. The positron number density per unit energy f obeys the diffusion-loss equation [37] [41]:

$$\frac{\partial f}{\partial t} - \nabla(\mathcal{K}(E_{e^+}, \vec{x}) \nabla f) - \frac{\partial}{\partial E_{e^+}}(b(E_{e^+}, \vec{x}) f) = Q(E_{e^+}, \vec{x}) \quad (3.10)$$

where $\mathcal{K}(E_{e^+}, \vec{x})$ is the diffusion coefficient function which describe transport through the turbulent magnetic fields. We adopt the customary parameterization $\mathcal{K} = \mathcal{K}_0 (E_{e^+}/\text{GeV})^\delta = \mathcal{K}_0 \epsilon^\delta$ with the parameters $\mathcal{K}_0 = 0.0112 \text{ kpc}^2/\text{Myr}$ and $\delta = 0.70$, which would result in a median final result [37]. $b(E_{e^+}, \vec{x})$ is the energy loss coefficient function which describes the energy loss due to several processes, such as synchrotron radiation and Inverse Compton scattering (ICS) off CMB photons, and/or infrared and optical galactic starlight, it is provided numerically by PPPC 4 DM ID [37] in the form of MATHEMATICA[®] interpolating functions. Q is the source term which can be expressed as

$$Q = \frac{\rho(r)}{m_\varphi} \sum_l \Gamma_l \frac{dN_{e^+}^l}{dE_{e^+}}. \quad (3.11)$$

Eq. 3.10 is solved in a cylinder that sandwiches the galactic plane with height $2L$ and radius $R = 20 \text{ kpc}$. The distance between the solar system and the galactic center is 8.33

kpc. Conditions electrons/positrons could escape freely are adopted on the surface of the cylinder. The resulting differential flux of positrons in the Solar System is

$$\frac{d\Phi_{e^+}}{dE_{e^+}}(E_{e^+}, r_\odot) = \frac{v_{e^+}}{4\pi b(E_{e^+}, r_\odot)} \frac{\rho_\odot}{m_\varphi} \sum_l \Gamma_l \int_{E_{e^+}}^{m_\varphi/2} dE_s \frac{dN_{e^+}^l}{dE_{e^+}}(E_s) I(E_{e^+}, E_s, r_\odot) \quad (3.12)$$

where r_\odot is the distance between the Solar System and the Galactic Center, and ρ_\odot is the DM density at the Solar System. E_s is the positron energy at production (s stands for "source"), $I(E_{e^+}, E_s, r_\odot)$ is the generalized halo function, which is the Green function from a source with positron energy E_s to any energy E_{e^+} , and it is also provided numerically by PPPC 4 DM ID [37] in the form of MATHEMATICA[®] interpolating functions.

The calculation of gamma rays consists of three parts, direct ("prompt") decay from the Milky Way halo, extragalactic gamma rays emitted by DM decay and gamma rays from Inverse Compton scattering (ICS). The synchrotron radiation is in a significant amount from where the magnetic field and the DM are very dense, close to the Galactic Center. This work focuses on high galactic latitude ($|b| > 20^\circ$), where the magnetic field is very weak, so synchrotron radiation is not included in this work.

The differential flux of photons from prompt decay of the Milky Way halo is calculated via

$$\frac{d\Phi_\gamma}{dE_\gamma d\Omega} = \frac{r_\odot \rho_\odot}{4\pi m_\varphi} \bar{J} \sum_l \Gamma_l \frac{dN_\gamma^l}{dE_\gamma} \quad (3.13)$$

where $\bar{J}(\Delta\Omega) = \int_{\Delta\Omega} J d\Omega / \Delta\Omega$ is the averaged J factor of the region of interest, $J = \int_{\text{l.o.s.}} \rho(r(s, \theta)) / (r_\odot \rho_\odot) ds$, $r(s, \theta) = (r_\odot^2 + s^2 - 2r_\odot s \cos\theta)^{1/2}$ is the distance between the DM and the Galactic Center, and θ is the angle between the direction of the line of sight (l.o.s.) and the line connecting the Sun to the Galactic Center.

The extragalactic gamma rays received at a point with redshift z is calculated via [37]

$$\frac{d\Phi_{\text{EG}\gamma}}{dE_\gamma}(E_\gamma, z) = \frac{c}{E_\gamma} \int_z^\infty dz' \frac{1}{H(z')(1+z')} \left(\frac{1+z}{1+z'}\right)^3 \frac{1}{4\pi} \frac{\bar{\rho}(z')}{m_\varphi} \sum_l \Gamma_l \frac{dN_\gamma^l}{dE_\gamma'}(E_\gamma') e^{-\tau(E_\gamma', z, z')} \quad (3.14)$$

where $H(z) = H_0 \sqrt{\Omega_m(1+z)^3 + (1-\Omega_m)}$ is the Hubble function, $\bar{\rho}(z) = \bar{\rho}_0(1+z)^3$ is the average cosmological DM density and $\bar{\rho}_0 \simeq 1.15 \times 10^{-6} \text{ GeV/cm}^3$, $E_\gamma' = E_\gamma(1+z')$, $\tau(E_\gamma', z, z')$ is the optical depth, which is also provided numerically by PPPC 4 DM ID [37] in the form of MATHEMATICA[®] interpolating functions. $\tau(E_\gamma', z, z')$ describes the absorption of gamma rays in the intergalactic medium between the redshifts z and z' . The presence of ultraviolet (UV) background lower the UV photon densities. There are three absorption models provided by PPPC 4 DM ID [37], (no ultraviolet (noUV), minimal ultraviolet (minUV) and maximal ultraviolet (maxUV)). We calculated the Hubble function in the Λ CDM cosmology with a pressure-less matter density of the universe $\Omega_m = 0.27$, dark energy density of the universe $\Omega_\Lambda = 0.73$ and scale factor for Hubble expansion rate 0.7.

Galactic electrons/positrons generated by ssDM could lose their energy into photons by means of the inverse Compton scattering. The greater the mass of ssDM is, the higher

the energy of the electrons/positrons generated by ssDM is, and the more important this effect is. The inverse Compton gamma rays is calculated as follows,

$$\frac{d\Phi_{\text{IC}\gamma}}{dE_\gamma d\Omega} = \frac{1}{E_\gamma^2} \frac{r_\odot}{4\pi} \frac{\rho_\odot}{m_\varphi} \int_{m_e}^{m_\varphi/2} dE_s \sum_i \Gamma_i \frac{dN_{e^+}^i}{dE}(E_s) I_{\text{IC}}(E_\gamma, E_s, b, l) \quad (3.15)$$

where b and l is the galactic latitude and galactic longitude respectively, $I_{\text{IC}}(E_\gamma, E_s, b, l)$ is a halo function for the IC radiative process, which is also provided numerically by PPPC 4 DM ID [37] in the form of MATHEMATICA[®] interpolating functions.

4 Constraints from isotropic diffuse γ -ray background (IGRB) and the cosmic positron spectrum

4.1 Statistic methods to set constraints

The isotropic diffuse γ -ray background is measured by Fermi-LAT [32]. We compared the γ -ray flux produced by DM with IGRB to set constraints on the lifetime of ssDM. The region of interest in our work only includes high-latitude regions ($|b| > 20^\circ$) because the analysis of the IGRB by Fermi-LAT only includes high-latitude ($|b| > 20^\circ$) [32], where b is the galactic latitude.

The cosmic positron flux is measured by the AMS on the International Space Station [33]. We also compared the positron flux produced by DM with the measured flux to set constraints on the lifetime of ssDM.

The comparison strategies used in this paper are as follows. Define χ^2 as

$$\chi^2 = \sum_i \frac{(\Phi_i^{\text{th}} - \Phi_i^{\text{obs}})^2}{\delta_i^2} \Theta(\Phi_i^{\text{th}} - \Phi_i^{\text{obs}}) \quad (4.1)$$

where Φ_i^{th} and Φ_i^{obs} denote the predicted and observed fluxes respectively, δ_i are the experimental errors, and $\Theta(x)$ is the Heaviside function. This work require $\chi^2 < 9$ to obtain an approximate estimate of 3- σ constraint [39] [40] and only energy bins located at above 1 GeV are used.

4.2 Treatment of the background

The IGRB could be contributed by many unresolved sources, such as non-blazar active galactic nuclei, the unresolved star-forming galaxies, BL Lacs, flat-spectrum radio quasar blazars and electromagnetic cascades generated through ultra-high energy cosmic-ray propagation. When the IGRB is used to constrain the lifetime of DM, some work takes the contribution of these sources into account, so they could get the most stringent constraints [38]. On the contrary, some work did not take the contribution of these sources into account, so they could get conservative constraints [40]. In our work, we adopt the latter case that those contributions are not added in the total flux, so the results we obtained would also be very conservative.

Similar to the IGRB case, it is usually believed that the cosmic positron spectrum has a power-law background. We also do not take into account this contribution in the total predicted flux, so the results obtained by using the cosmic positron flux would also be very conservative.

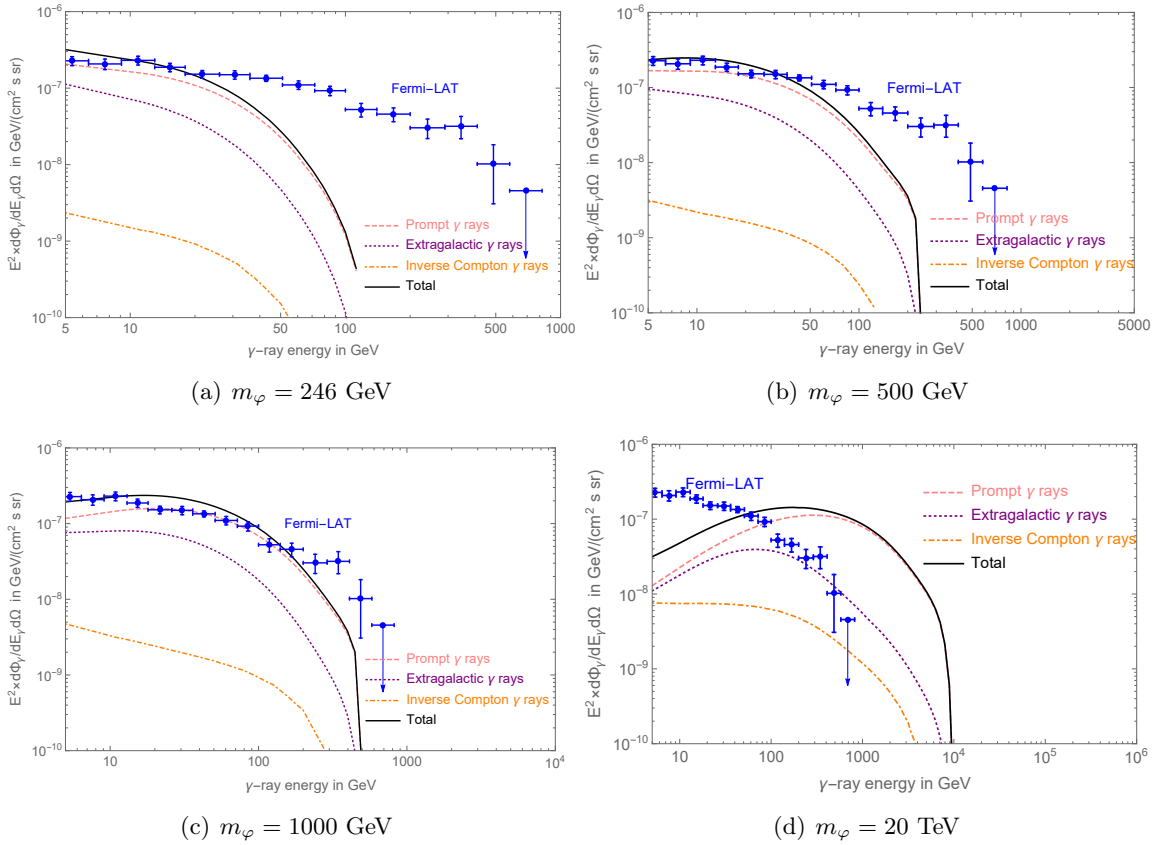


Figure 2. Averaged photon fluxes ($|b| > 20^\circ$) from decaying DMPs of prompt emission component, extragalactic component, and inverse Compton scattering component are shown by the dashed line, dotted line and dot-dashed line respectively when $\tau = 5.3 \times 10^{26} s$. The total flux of these three components is shown by the black solid line. Fermi-LAT observations of the IGRB are also plotted by blue points with error bars.

5 Results

Based on the procedure outlined in Section 3, the photon flux and the positron flux arising from DMP decay, and which would be detected by satellites, were calculated.

Fig. 2 shows the averaged photon flux ($|b| > 20^\circ$) from decaying DMPs of prompt emission component, extragalactic component, inverse Compton scattering component, and the total flux when the lifetime of ssDM is $\tau = 5.3 \times 10^{26} s$ and the minUV model is adopted. It can be seen from Fig. 2(a)-(c) that when $v < m_\phi < 1000$ GeV, prompt photon flux contributed main part of the total flux, and the contribution of inverse Compton scattering is the least. When the mass of ssDM is large enough (e.g. $m_\phi = 20$ TeV as shown in Fig. 2(d)), the contribution from inverse Compton scattering in the low energy region of the photon spectrum is comparable with the prompt emission component and the extragalactic component.

Fig. 3 show the averaged photon flux ($|b| > 20^\circ$) from decaying DMPs contributed by

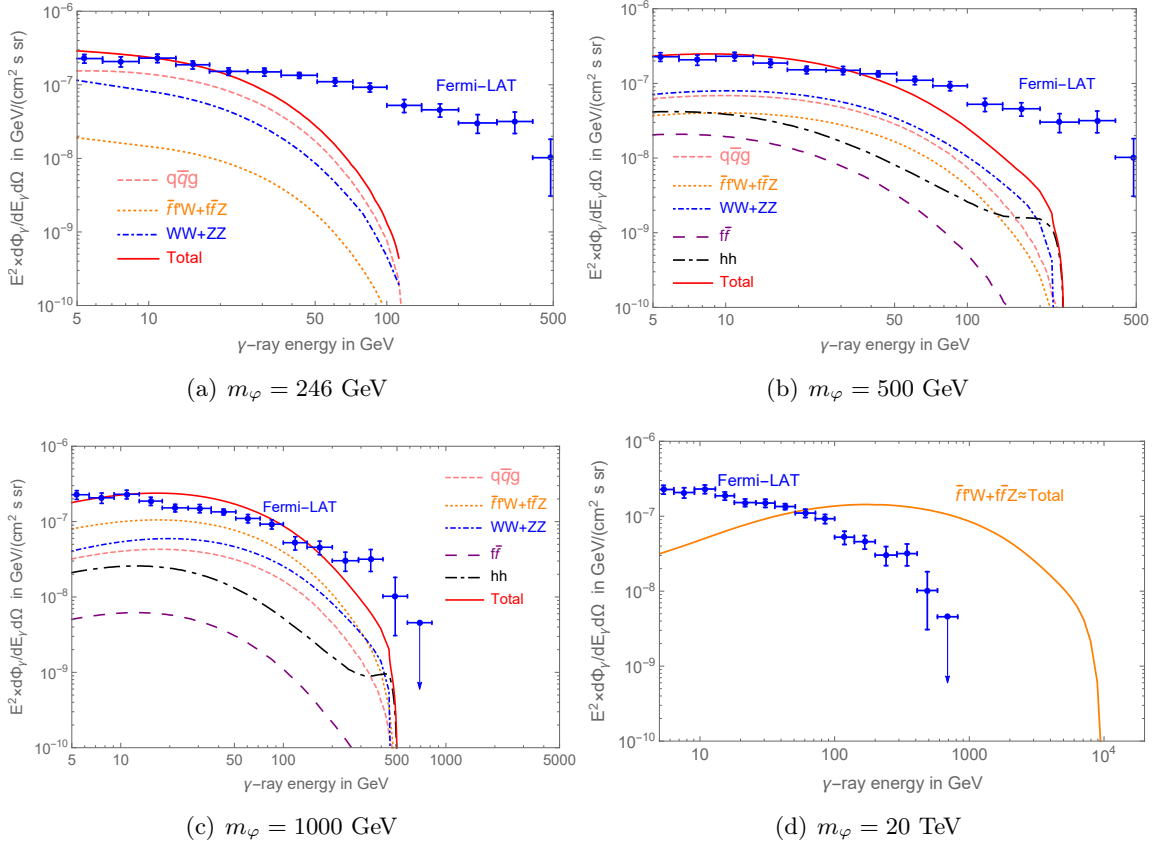


Figure 3. Averaged photon flux ($|b| > 20^\circ$) from decaying DMPs contributed by various channels are shown when $\tau = 5.3 \times 10^{26} s$. The total flux is shown by the solid line. Fermi-LAT observations of the IGRB are also shown by blue points with error bars.

different channels when $\tau = 5.3 \times 10^{26} s$ and the minUV model is adopted. It can be seen from Fig. 3(a)–(c) that when $v < m_\varphi < 1000$ GeV, two-body decays are of comparable contributions with the three-body channels. This result is consistent with Fig. 1 that when $v < m_\varphi < 1000$ GeV, the branching ratio of two-body decays are of comparable contributions with the three-body channels. Among all the channels, the $\varphi \rightarrow h, h$ channel is more characteristic, its contribution to the photon flux increases slightly near the cut-off. When the mass of the DM particle is $m_\varphi = 20$ TeV, it could be seen from Fig. 3(d) that most of the photons comes from the $\varphi \rightarrow \bar{f}f'W + \bar{f}fZ$ channel. This result is also consistent with Fig. 1 that when $4\pi v \lesssim m_\varphi \lesssim 10^5$ GeV, the branching ratio of ssDM is dominated by the same channel.

Fig. 4 shows the absorption of UV photons with the presence of the UV background compared with no UV background regime when $\tau = 5.3 \times 10^{26} s$. When $v < m_\varphi < 1000$ GeV, comparing the maximum of these discrepancies as shown in Fig. 4(a)–(c) with the total flux shown in Fig. 2(a)–(c) or Fig. 3(a)–(c), we have $(\Delta\Phi/\Phi)_{\max} \sim 10^{-2}$. When the mass of ssDM is $m_\varphi = 20$ TeV, comparing the maximum of the discrepancy as shown in Fig. 4(d) with the total flux shown in Fig. 2(d) or Fig. 3(d), we have $(\Delta\Phi/\Phi)_{\max} \sim 10^{-1}$.

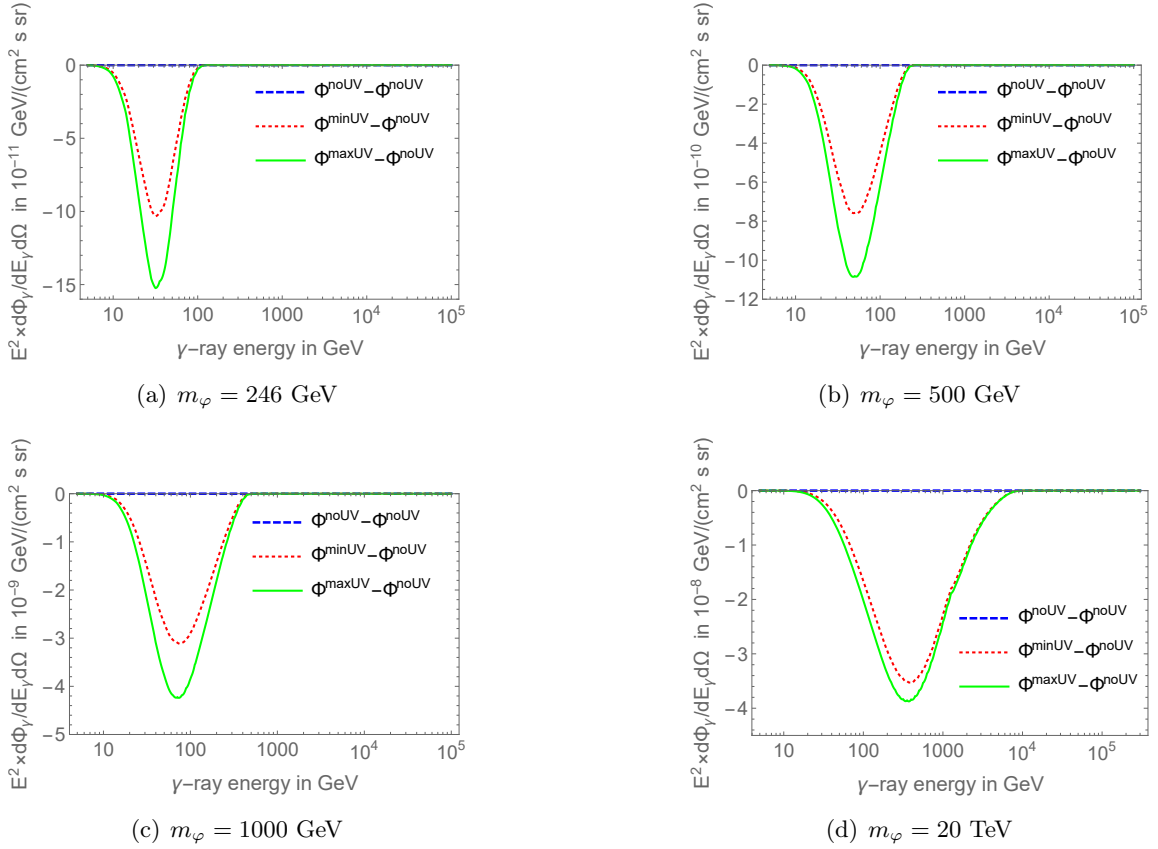


Figure 4. The presence of UV background lower the UV photon densities. The figure shows the absorption of UV photons compared with no UV background regime when $\tau = 5.3 \times 10^{26}$ s.

These results show that the absorption from the UV background becomes apparent, when the mass of the DM particles is large.

Fig. 5 show the positron flux from decaying DMPs contributed by various channels when $\tau = 10^{26}$ s. Fig. 5(a) shows that when $m_\varphi = v$, three-body decays tends to contribute positrons in the low energy region, while $\varphi \rightarrow WW + ZZ$ channel tends to contribute positrons in high energy region. It could be infer from Fig. 5(b) and 5(c) that when $500 \text{ GeV} < m_\varphi < 1000 \text{ GeV}$, two-body decays are of comparable contributions with the three-body channels. Similar to the photon case, this result is consistent with Fig. 1 that when $500 \text{ GeV} < m_\varphi < 1000 \text{ GeV}$, the branching ratio of two-body decays are of comparable contributions with the three-body channels. When the mass of the DM particle is $m_\varphi = 20 \text{ TeV}$, it could be seen from Fig. 5(d) that most of the positrons comes from the $\varphi \rightarrow \bar{f}f'W + \bar{f}f'Z$ channel. As expected, this result is consistent with Fig. 1 that when $4\pi v \lesssim m_\varphi \lesssim 10^5 \text{ GeV}$, the branching ratio of ssDM is dominated by the same channel.

Based on the procedure outlined in Section 4, the excluded two-dimensional parameter space (τ, m_φ) is shown in Fig. 6, where minUV model is adopted. The shadowed area below the dashed line is the excluded region of parameter space (τ, m_φ) as constrained by Fermi-

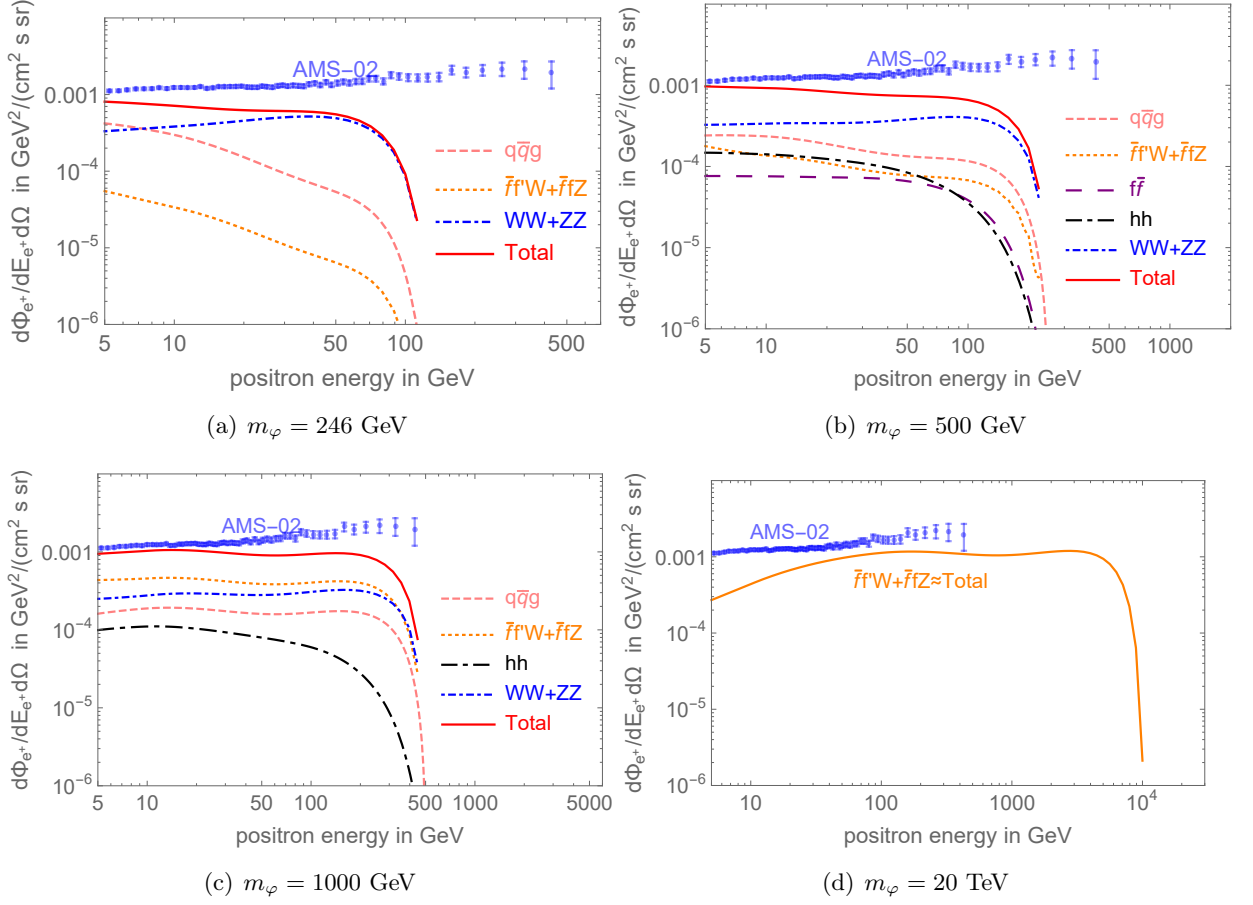


Figure 5. Predicted positron flux from decaying DMPs contributed by various channels are shown when $\tau = 10^{26}$ s. The total flux is shown by the solid line. AMS-02 observations of positron flux are also shown by blue points with error bars [33].

LAT. The shadowed area below the dotted line is the parameter space (τ, m_φ) excluded by AMS-02. For comparison, a conservative excluded parameter space from observations of the cosmic neutrino flux [16] [23] is shown by the shadowed area above the dot-dashed line. Besides, we also plotted the line for $\Lambda_{EW} = 246$ GeV, which represents the typical energy of the electroweak scale. It is clear that when the mass of the DMP is around the electroweak scale, ssDM lifetime smaller than 5.3×10^{26} s can be excluded. Since ξ reveals the influence of gravity on the global symmetry of ssDM, the excluded region of parameter space (ξ, m_φ) is given in Fig. 7, where minUV model is adopted.

6 Discussion and Conclusions

Global symmetry can guarantee the stability of ssDM particles. However, the nonminimal coupling between ssDM and gravity can destroy their global symmetry, hence leading to their decay.

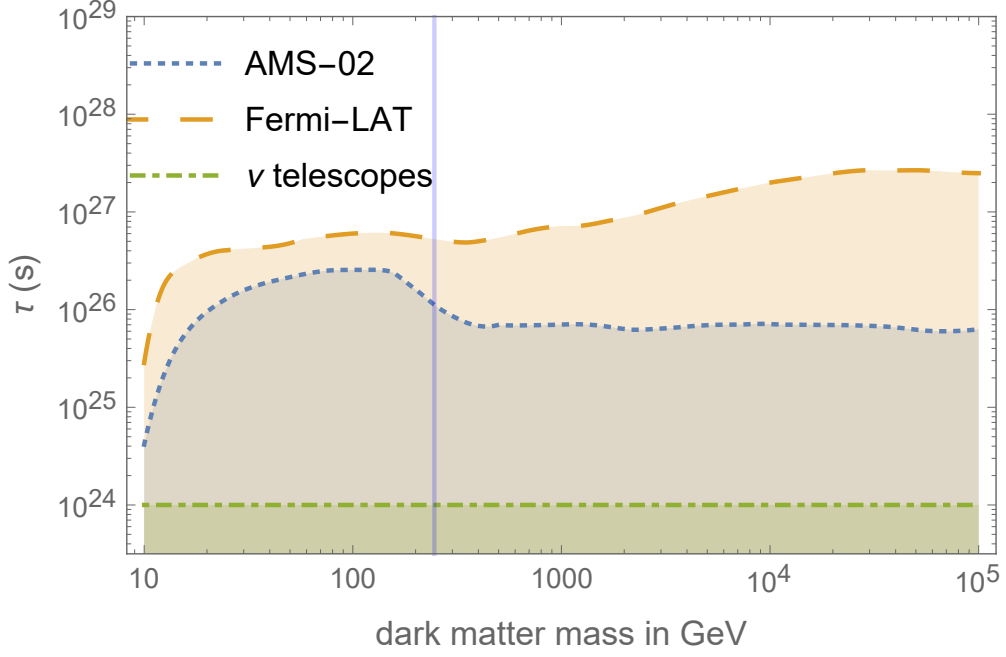


Figure 6. The $\tau - m_\varphi$ plane. The shadowed regions are regions excluded by observation of the IGRB by Fermi-LAT and the cosmic-ray positron spectrum obtained by AMS-02. For comparison, the conservative excluded parameter space from observations of the cosmic neutrino flux [16] [23] is shown by the shadowed area below the dot-dashed line.

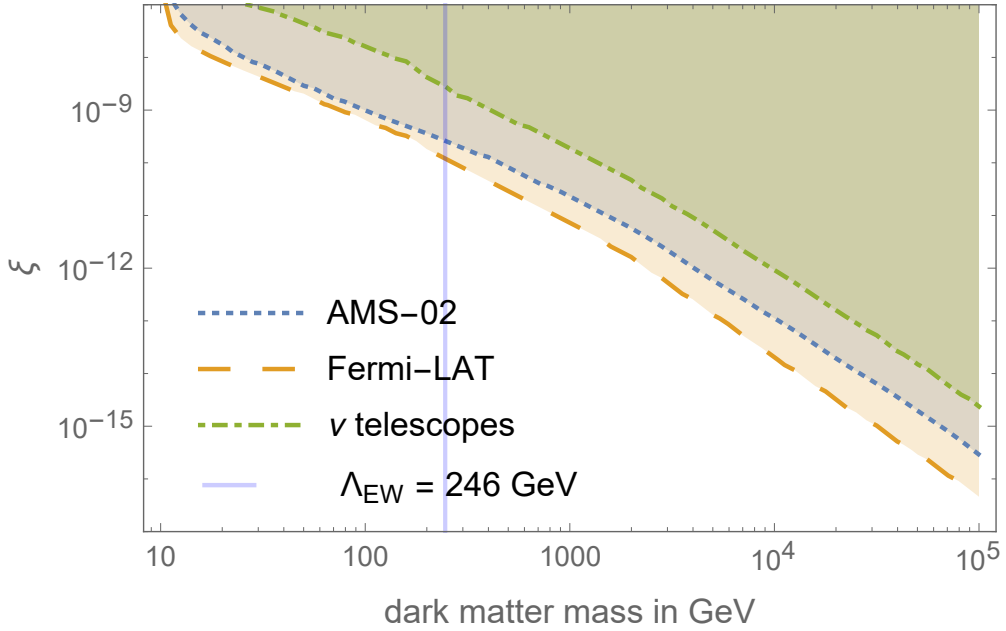


Figure 7. The $\xi - m_\varphi$ plane. The shadowed regions are regions excluded by observation of the IGRB by Fermi-LAT and the cosmic-ray positron spectrum obtained by AMS-02. For comparison, a conservative excluded parameter space from observations of the cosmic neutrino flux [16] [23] is shown by the shadowed area above the dot-dashed line.

In this study, we set constraints on the lifetime and the symmetry breaking strength of ssDM particles using the most sensitive observations of photons and cosmic rays respectively made by Fermi-LAT and AMS-02. The results in Fig. 7 show that the non-minimal coupling constant between the Ricci scalar and the ssDM receives a stronger limitation from indirect detection when the mass of ssDM is larger. This behaviour is attributed to the fact that an ssDM particle with a larger mass has more decay channels and larger phase space. And it confirms Catà et al.'s conclusion in GeV–TeV range that the exclusion of large regions of the parameter spaces means an additional stabilizing symmetry should be in place.

Different from the previous work by [30], the mass range of ssDM particles considered in our study is around the GeV–TeV range. Near this scale, the decay channels are more abundant and the phase space is larger. In the work by Catà et al. [30], the lifetime of an ssDM candidate with mass around $m_\varphi \gtrsim 1$ MeV decaying through a gravity portal is constrained to $\tau \gtrsim 10^{24} - 10^{26}$ s. In this work, the lifetime of ssDM smaller than 5.3×10^{26} is excluded at $3\text{-}\sigma$ confidence level when the mass of the ssDM is around the electroweak scale (246 GeV). The mass region analyzed here contains abundant decay channels that the MeV scale doesn't have, so the analysis of the decay properties are more comprehensive.

What is going on in parallel with this work is a new paper on this topic¹, which points out that the fermionic fields should be conformally rescaled in the Einstein Frame. In their regime, all the vertices containing only one gauge boson disappear. Meanwhile, the decay rate of all other channels, including the $\varphi \rightarrow \bar{f}_i, f_i$ channels, remains unchanged at tree level. Consequently, in the vicinity of the interested electroweak scale ($v < m_\varphi < 1000$ GeV), the constraints from IGRB on ξ and lifetime is still in the same order of magnitude compared with our scenario. However, in the region deviating from the electroweak scale ($m_\varphi < v$ and 10^3 GeV $< m_\varphi < 10^5$ GeV), the constraints from IGRB on ξ and lifetime is significantly weakened.

The DAMPE detector was designed to run for at least three years, and the energies measured in the future may be up to about 10 TeV [34]. The Large High Altitude Air Shower Observatory (LHAASO) also will be able to detect γ -ray signals from DM particles of PeV-EeV masses decaying on the time scale up to 3×10^{29} s.² These missions suggest that future data obtained by DAMPE and LHAASO can be used to further investigate the impact of gravity on the global symmetry of DM.

References

- [1] Gianfranco Bertone, *Particle Dark Matter: Observations, Models and Searches*, (Cambridge Univ. Press, Cambridge, 2010)
- [2] C. Patrignani et al. (**Particle Data Group**), *Review of Particle Physics*, *Chin. Phys. C* **40** (2016) 100001.
- [3] Maxim Yu. Khlopov, *Probes for dark matter physics*, *Int. J. Mod. Phys. D* **27** (2018) 1841013. [arxiv:1802.10184](https://arxiv.org/abs/1802.10184)

¹F. Bezrukov et al., arXiv:2006.03431

²A. Neronov, D. Semikoz, arXiv:2001.11881

- [4] Maxim Khlopov, *Cosmoparticle physics of dark matter*, *EPJ Web Conf.* **222** (2019) 01006. [arxiv:1910.12910v1](#)
- [5] Thomas Hambye, *On the stability of particle dark matter*, *PoS IDM2010* (2011) 098. [arxiv:1012.4587](#)
- [6] K. Belotsky, M. Khlopov, C. Kouvaris, and M. Laletin, *Decaying Dark Atom Constituents and Cosmic Positron Excess*, *Adv. High Energy Phys.* **2014** (2014) 214258. [arxiv:1403.1212](#)
- [7] K. Belotsky, M. Khlopov, C. Kouvaris, and M. Laletin, *High Energy Positrons and Gamma Radiation from Decaying Constituents of a two-component Dark Atom Model*, *Int. J. Mod. Phys. D* **24** (2015) 1545004. [arxiv:1508.02881](#)
- [8] John McDonald, *Gauge singlet scalars as cold dark matter*, *Phys. Rev. D* **50** (1994) 3637-3649.
- [9] Vanda Silveira and A. Zee, *Scalar Phantoms*, *Phys. Lett. B* **161** (1985) 136-140.
- [10] Tom Banks and Nathan Seiberg, *Symmetries and strings in field theory and gravity*, *Phys. Rev. D* **83** (2011) 084019. [arxiv:1011.5120](#)
- [11] Renata Kallosh, Andrei Linde, Dmitri Linde, and Leonard Susskind, *Gravity and global symmetries*, *Phys. Rev. D* **52** (1995) 912-935. [arxiv:hep-th/9502069](#)
- [12] V. Berezhinsky, Anjan S. Joshipura, and José W. F. Valle, *Gravitational violation of R parity and its cosmological signatures*, *Phys. Rev. D* **57** (1998) 147-151. [arxiv:hep-ph/9608307](#)
- [13] Eduard Massó, Francesc Rota, and Gabriel Zsembinski, *Planck-scale effects on global symmetries: Cosmology of pseudo-Goldstone bosons*, *Phys. Rev. D* **70** (2004) 115009. [arxiv:hep-ph/0404289](#)
- [14] Sofiane M. Boucenna, Roberto A. Lineros and José W.F. Valle, *Planck-scale effects on WIMP dark matter*, *Front.in Phys.* **1** (2014) 34. [arxiv:1204.2576](#)
- [15] Yann Mambrini and Stefano Profumo and Farinaldo S. Queiroz, *Dark matter and global symmetries*, *Phys. Lett.* **B760** (2016) 807-815. [arxiv:1508.06635](#)
- [16] O. Catà, A. Ibarra, and S. Inghenütt, *Dark Matter Decays from Nonminimal Coupling to Gravity*, *Phys. Rev. Lett.* **117** (2016) 021302. [arxiv:1603.03696](#).
- [17] Fedor Bezrukov and Mikhail Shaposhnikov, *The Standard Model Higgs boson as the inflaton*, *Phys. Lett. B* **659** (2008) 703-706. [arxiv:0710.3755](#)
- [18] Soo-Min Choi, Yoo-Jin Kang, Hyun Min Lee and Kimiko Yamashita, *Unitary inflaton as decaying dark matter*, *JHEP* **05** (2019) 060. [arxiv:1902.03781](#)
- [19] Gonzalo, Alonso-Álvarez and Joerg Jaeckel, *Lightish but clumpy: scalar dark matter from inflationary fluctuations*, *JCAP* **10** (2018) 022. [arxiv:1807.09785](#)
- [20] Catarina Cosme, João G. Rosa and O. Bertolami, *Scale-invariant scalar field dark matter through the Higgs portal*, *JHEP* **05** (2018) 129. [arxiv:1802.09434](#)
- [21] Wei Cheng and Ligong Bian, *From inflation to cosmological electroweak phase transition with a complex scalar singlet*, *Phys. Rev. D* **98** (2018) 023524. [arxiv:1801.00662](#)
- [22] Wei Cheng, Ligong Bian, *From inflation to cosmological electroweak phase transition with a complex scalar singlet*, *Phys. Rev. D* **99** (2019) 035038. [arxiv:1805.00199](#)
- [23] O. Catà, A. Ibarra, and S. Inghenütt, *Dark matter decay through gravity portals*, *Phys. Rev. D* **95** (2017) 035011. [arxiv:1611.00725v2](#)

- [24] Eric Armengaud, *Direct detection of WIMPs*, *C. R. Phys.* **13** (2012) 730-739.
- [25] Jan Conrad and Olaf Reimer, *Indirect dark matter searches in gamma and cosmic rays*, *Nature Phys.* **13** (2017) 224-231. [arxiv:1705.11165](#)
- [26] Gaëlle Giesen, Mathieu Boudaud, Yoann Génolini, Vivian Poulin, Marco Cirelli, Pierre Salati and Pasquale D. Serpico, *AMS-02 antiprotons, at last! Secondary astrophysical component and immediate implications for Dark Matter*, *JCAP* **09** (2015) 023. [arxiv:1504.04276](#)
- [27] M.G. Aartsen et al. (**IceCube** Collaboration), *Search for Dark Matter Annihilations in the Sun with the 79-String IceCube Detector*, *Phys. Rev. Lett.* **110** (2013) 7. [arxiv:1212.4097](#)
- [28] M. Ackermann et al. (The **Fermi-LAT** Collaboration), *Searching for Dark Matter Annihilation from Milky Way Dwarf Spheroidal Galaxies with Six Years of Fermi Large Area Telescope Data*, *Phys. Rev. Lett.* **115** (2015) 231301. [arxiv:1503.02641](#)
- [29] Gianfranco Bertone and Tim M. P. Tait, *A new era in the search for dark matter*, *Nature* **562** (2018) 51-56.
- [30] O. Catà, A. Ibarra, and S. Inghenütt, *Sharp spectral features from light dark matter decay via gravity portals*, *JCAP* **11** (2017) 044. [arxiv:1707.08480](#).
- [31] Feng and Jonathan L., *Dark Matter Candidates from Particle Physics and Methods of Detection*, *Ann. Rev. Astron. Astrophys.* **48** (2010) 495-545. [arxiv:1003.0904](#).
- [32] M. Ackermann et al., *The spectrum of isotropic diffuse gamma-ray emission between 100 MeV and 820 GeV*, *Astrophys. J.* **799(1)** (2015) 86. [arxiv:1410.3696](#).
- [33] M. Aguilar et al. (**AMS** Collaboration), *Electron and Positron Fluxes in Primary Cosmic Rays Measured with the Alpha Magnetic Spectrometer on the International Space Station*, *Phys. Rev. Lett.* **113** (2014) 121102. [arxiv:1701.07305](#).
- [34] G. Ambrosi et al. (**DAMPE** Collaboration), *Direct detection of a break in the teraelectronvolt cosmic-ray spectrum of electrons and positrons*, *Nature* **552** (2017) 63-66. [arxiv:1711.10981](#)
- [35] Jing Ren, Zhong-Zhi Xianyu and Hong-Jian He, *Higgs gravitational interaction, weak boson scattering, and Higgs inflation in Jordan and Einstein frames*, *JCAP* **1406** (2014) 032. [arxiv:1404.4627](#)
- [36] M. Tanabashi et al. (**Particle Data Group**), *Review of Particle Physics*, *EPJ C* **98** (2018) 030001.
- [37] M. Cirelli, G. Corcella, A. Hektor, G. Hütsi, M. Kadastik, P. Panci, M. Raidal, F. Sala and A. Strumia, *PPPC 4 DM ID: a poor particle physicist cookbook for dark matter indirect detection*, *JCAP* **03** (2011) 051. [arxiv:1012.4515](#)
- [38] C. Blanco and D. Hooper, *Constraints on decaying dark matter from the isotropic gamma-ray background*, *JCAP* **03** (2019) 019. [arxiv:1811.05988](#)
- [39] O. Kalashev, *Constraining Dark Matter and Ultra-High Energy Cosmic Ray Sources with Fermi-LAT Diffuse Gamma Ray Background*, *EPJ Web Conf.* **125** (2016) 02012. [arxiv:1608.07530](#)
- [40] L. Wei, X.-J. Bi, S.-J. Lin and P.-F. Yin, *Constraints on dark matter annihilation and decay from the isotropic gamma-ray background*, *Chin. Phys. C* **41** (2017) 045104. [arxiv:1602.01012](#)
- [41] T. Delahaye et al., *Galactic secondary positron flux at the Earth*, *Astron. Astrophys.* **501** (2009) 821. [arxiv:0809.5268](#)